Research Paper

A fully coupled thermo-poro-mechanical finite element analysis to predict the thermal pressurization and thermally induced pore fluid flow in soil media

Mohammadreza Mir Tamizdoust, Omid Ghasemi-Fare*

Department of Civil and Environmental Engineering, University of Louisville, USA

ABSTRACT

Temperature gradient and heat transfer in saturated porous media may affect pore fluid pressure and/or pore fluid flow depending on thermal, mechanical, and hydraulic properties of the media and the saturating fluid. Therefore, several Thermo-hydro-mechanical (THM) models have been developed to theoretically analyze the thermal behavior of soil media. In this study a coupled thermo-poro-mechanical model is adopted to investigate the heat and mass transfer in deformable porous media in a transient and quasi-steady state conditions. The Effects and importance of different properties of porous media are carefully taken into account to simulate two different cases with different scenarios. The results confirm that in order to accurately predict the thermal pressurization and changes in total stress, temperature dependency of properties of the soil and saturating fluid must be considered carefully. It is found that even a slight perturbation in porosity variation and temperature dependency of the thermal expansion coefficient of the fluid can greatly influence the thermal pressurization of pore fluid in very low permeable soils (e.g. clays), while variations of pore fluid density governs thermally-induced pore fluid flow in high permeable soils (e.g. sands and silty sands). Moreover, the feasibility of heat convection and heat-induced pore fluid flow is discussed in a parametric study with different temperature and permeability values. The results demonstrate that the Boussinesq approximation is a key assumption when dealing with heat-induced pore fluid flow in quasi-steady state condition.

1. Introduction

Heat transfer mechanisms in fluid saturated porous media have been investigated in different scales from cavities [1–5] to hydro-thermal systems [6–13] within last four decades. Heat convection has been considered for large-scale hydrothermal problems such as magma intrusions in deep aquifers [6,10]. In such studies, heat and mass transport have been solved considering the Boussinesq approximation [14]. Boussinesq theorem assumes that the fluid density in heat and mass transfer equations is constant except in the gravitational force acting on the fluid. However, the validity of Boussinesq approximation is only acceptable in a quasi-steady state condition [10]. The utilization of the aforementioned approximation can be seen in natural heat convection problems [5,15,16]. Delaney [6] developed an analytical and numerical frameworks to simulate the pressurization and ground water flow in a host rock which is subjected to a sudden heating from the magma intrusion. He investigated the onset of hydrothermal convection in 0.1–5 km depths when temperature rises from 500 K to 1000 K. An

overview of the application and advances of numerical modeling of ground water flow subjected to heating and hydrothermal systems (e.g. magma intrusions) are presented by Anderson [9] and Ingebritsen et al. [10]. Recently, Townsend [11], extended the work of Delaney [6] to analyze the variations of porosity and permeability caused by mineral precipitation clogging the pores when the porous medium is subjected to instantaneous high temperature.

Depending on the nature of the problem, heat transfer may have profound coupling effects on pore fluid flow and/or pore fluid pressure. Several experimental and numerical research have been carried out to analyze the effects of thermal loading on hydraulic and mechanical properties of the porous media (e.g., soil) in transient and steady state conditions [17–24]. In the past two decades, thermo-poro-mechanical theory has been used to accurately predict the thermo-hydro-mechanical (THM) behavior of normally-consolidated and over-consolidated clays [20,25,26]. Thermo-elastoplastic constitutive models such as TEAM [27] and ACMEG-T [28] have been found to be useful in justi-fying the thermo-mechanical experimental studies on clays with

---
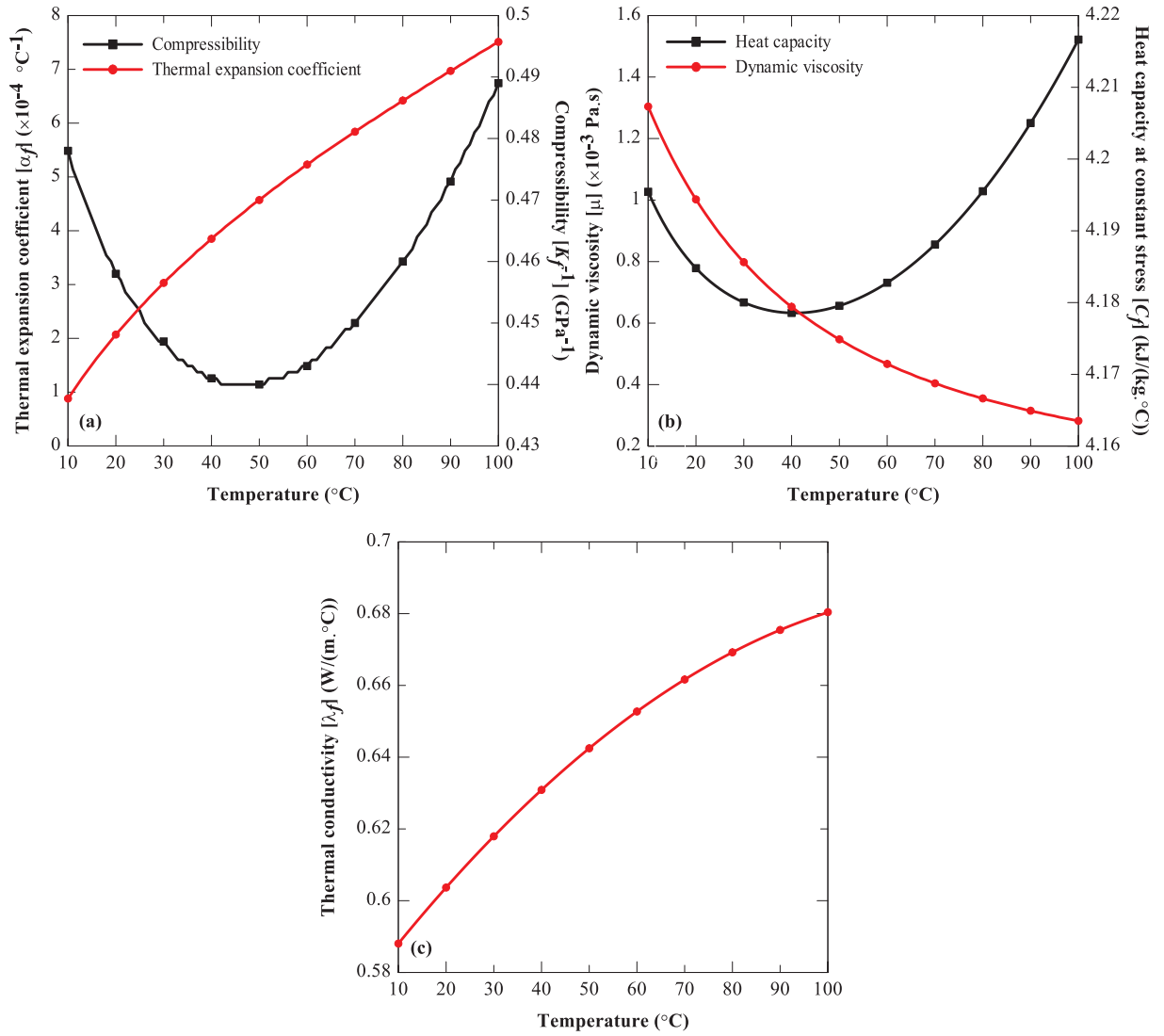
Fig. 1. The variations of physical properties of water with temperature at atmospheric pressure Spang [42]: (a) thermal expansion coefficient, and compressibility, (b) dynamic viscosity, and specific heat capacity, (c) thermal conductivity.
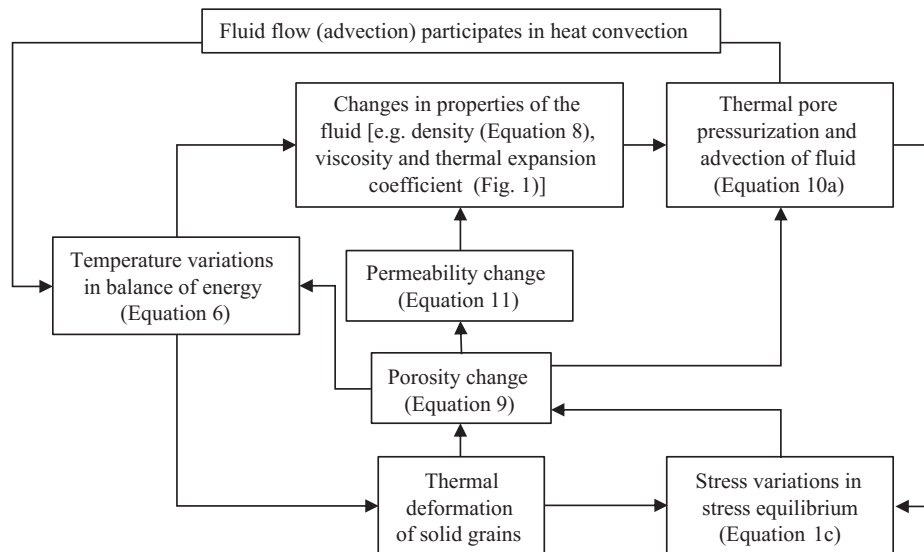
Fig 2. Flowchart of the fully coupled thermo-hydro-mechanical framework considered in this study.
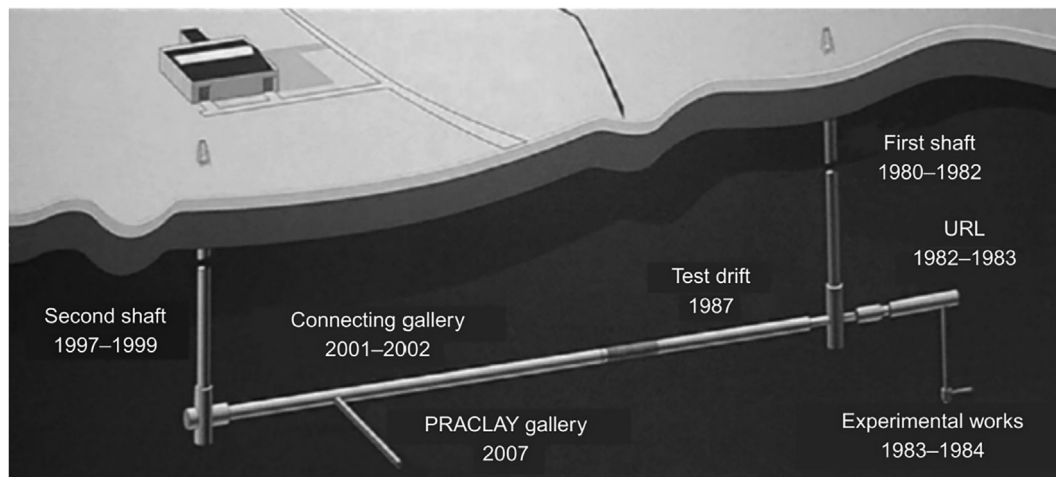
Fig. 3. Layout of the underground research facilities HADES-URF in Mol, Belgium [35].
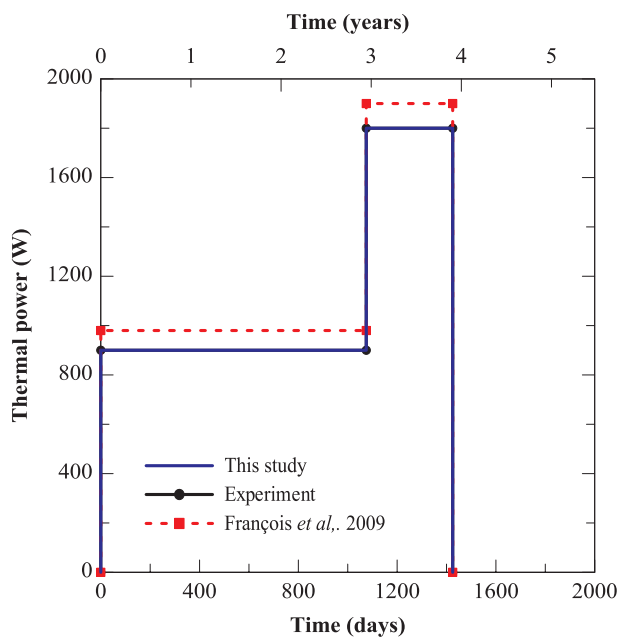

Fig. 4. Thermal loading at the heater level.

Table 1
Physical Properties of Boom clay.

Parameters (dimensions)	Values
ρ_{f0} (kg/m^3)	1000
ρ_s (kg/m^3)	2670
n_0	0.39
k_0 (m^2)	2.5×10^{-19}
E[a] (MPa)	350
ν	0.125
λ_s (W/m.°C)	1.65
C_s (J/kg.°C)	730
α_s (1/°C)	1.3×10^{-5}

[a] $K = E/3(1\text{-}2\nu)$.

Table 2
Initial condition of the field variables.

Parameters (dimensions)	Values
σ_z (MPa)	4.5
σ_r (MPa)	4.5
p_f (MPa)	2.025
OCR	2.4
T (°C)	16.5

different over-consolidation ratios.

In general, thermal loading can change hydraulic and mechanical features of the fluid saturated porous medium through altering the fluid density and porosity of the medium. Variations of fluid density and porosity in heat and mass transfer equations change the state of stress and induce deformation in the medium. Several researchers have studied the soil thermal response and reported changes in thermo-hydro or mechanical response of the soil during heat rejection and extraction from geothermal piles [21,29–32]. Much attention has been given to the transient heat transfer and temperature-induced pore fluid pressure in deep geological waste repositories due to the low permeability of clay [33,34]. Therefore, the effect of temperature-induced pore fluid flow, and consequently heat convection, has been overlooked even in high permeable soils (e.g. sands and silty sands) because of the fast dissipation of temperature-induced pore fluid pressure.

In order to accurately predict the stress state and deformation in porous media, the variations of fluid density and porosity should be considered in heat and mass transfer equations. Therefore, in this study, the magnitude and occurrence of heat-induced pore fluid pressure and/or heat-induced pore fluid flow are investigated with respect to different types of soil in transient and quasi-steady state conditions.

Moreover, fluid and soil properties (e.g., thermal expansion coefficient and dynamic viscosity of fluid) are considered to be temperature-dependent and are updated at each time step.

Two common heat sources in soil, (1) radioactive waste disposal and (2) energy pile, are considered in this study. A thermo-poro-mechanical model is adopted to predict the THM response of the soil media. The developed model is used to simulate the heat transfer and pore pressure generation in Boom clay surrounding a heat source deep into the soil. The results are compared with the in-situ measurements of the large-scale experiment called ATLAS in an underground research facility (HADES-URF) in Belgium [35]. Then, the validated model is used to analyze the onset and magnitude of heat-induced pore fluid flow and/or pore pressure to determine the threshold permeability in which heat-induced fluid flow happens considering different temperature and permeability values.

2. Theoretical formulation

The governing equations for the THM process are considered as stress equilibrium, mass balance, and energy balance of the medium. These three sets of coupled field equations are solved simultaneously by using COMSOL Multiphysics (COMSOL 5.3a). In the following section,
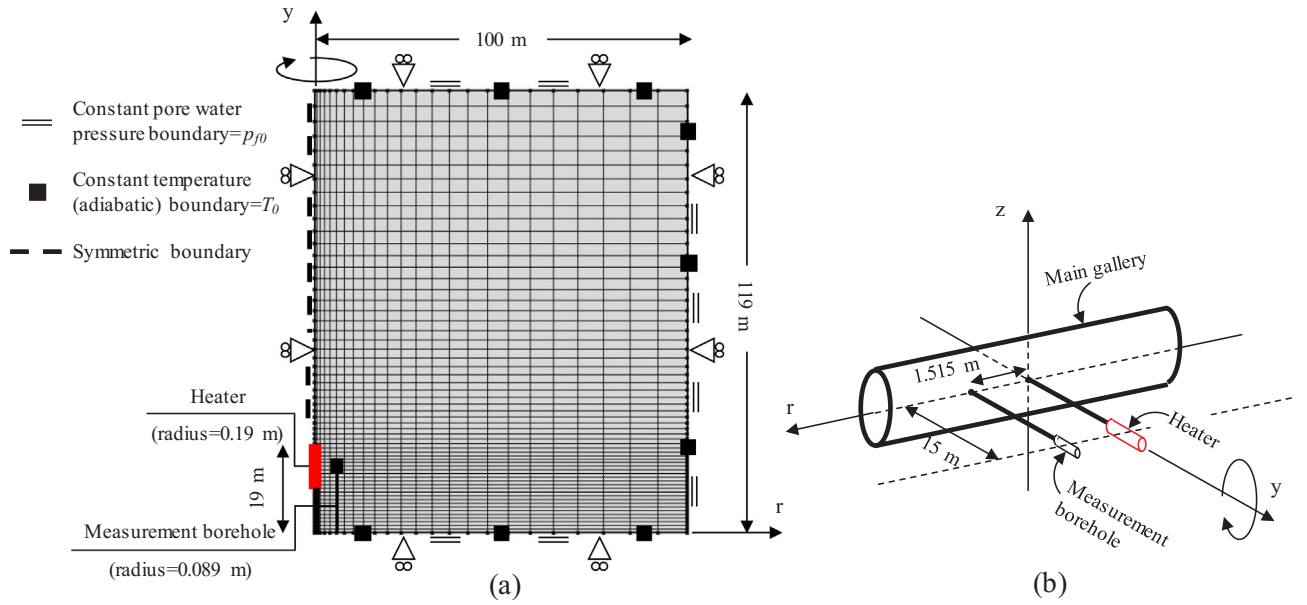
Fig. 5. (a) Finite element mesh of the domain with imposed boundary conditions and, (b) the 3D schematic view of ATLAS experiment.

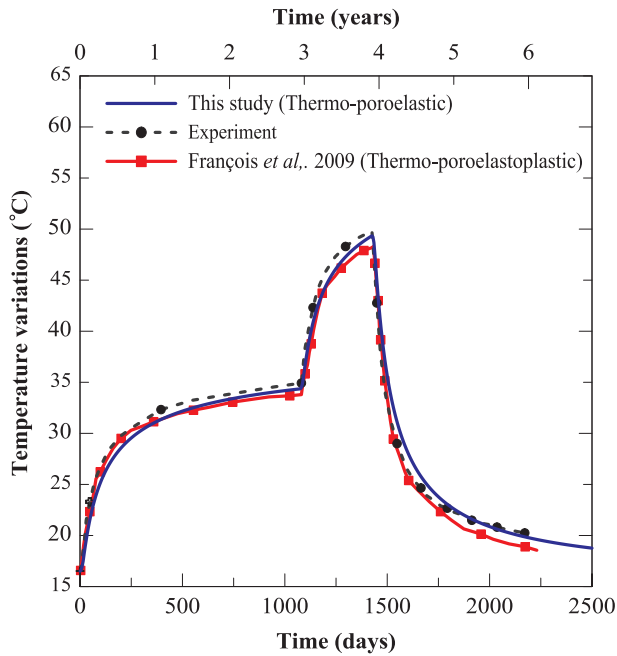**Fig. 6.** The evolution of temperature with time at the observation borehole (r = 1.515 m from the heater): The comparison between the current model with experiment and the Thermo-poroelastoplastic model [33].
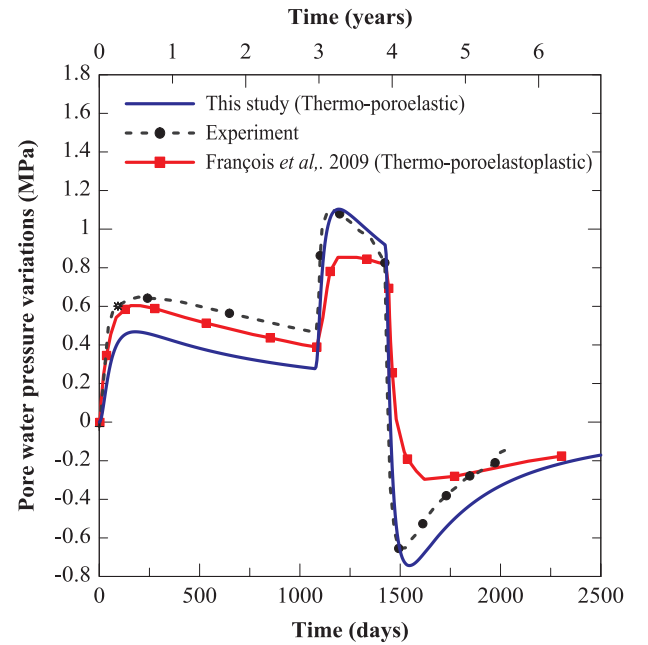

Fig. 7. The variation of thermal pressurization with time at the observation borehole (r = 1.515 m from the heater): The comparison between the current model, experiment and Thermo-poroelastoplastic model [33].

the governing partial differential equations considered in COMSOL Multiphysics are presented.

2.1. Macroscopic balance equations

A fluid (i.e. water) saturated deformable porous media is considered for this study. The porous medium is composed of incompressible solid grains with connected pores (no occluded porosity) filled with slightly compressible water. The solid and water phases are in thermal equilibrium; hence a unique temperature is assumed for the medium at each time step. The general soil stress equilibrium equation in cylindrical coordinate (r, φ, z) system is presented below:

$$\left(\frac{1}{r} \frac{\partial (r\sigma_r)}{\partial r} + \frac{1}{r} \frac{\partial \sigma_\varphi}{\partial \varphi} + \frac{\partial \sigma_z}{\partial z} \right) + \rho_m g = 0 \tag{1a}$$

$$\rho_m = n\rho_f + (1 - n)\rho_s \tag{1b}$$

where σ is total Cauchy stress tensor. ρ_m, ρ_f, and ρ_s are densities of medium, water, and solid grains, respectively; n is porosity and g is the acceleration of gravity.

In this study a 2D axisymmetric finite element modeling will be adopted due to the geometrical axisymmetric condition of the problems. In the first part of this study, a horizontal plane, where the temperature, pore pressure, and stress are measured on the same plane (ATLAS experiment) is considered. In the second part, thermal performance of a vertical heat source (e.g., energy pile) is simulated and
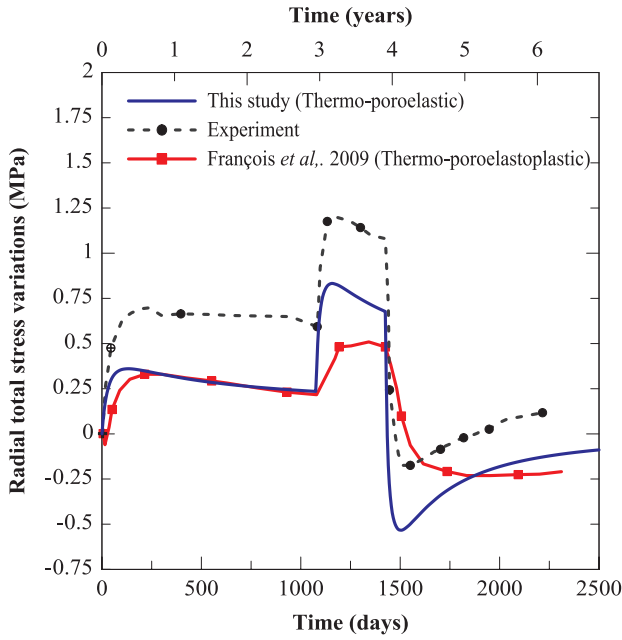
Fig. 8. The evolution of radial total stress with time at the observation borehole (r = 1.515 m from the heater): The comparison between the current model, experiment and Thermo-poroelastoplastic model [33].

therefore an axisymmetric vertical plane is considered. Since, the temperature difference at the pile surface around the pile in energy pile is lower than 2 °C [36] an axisymmetric vertical heat source can represent a geothermal heat exchanger pile [37]. In both conditions, the derivative of stress over azimuthal coordinate for axisymmetric plane (horizontal plane, and vertical plane, respectively for the first and second part of this study) is zero ($\partial \sigma_\varphi / \partial \varphi = 0$), therefore, Eq. (1a) can be replaced by Eq. (1c).

The soil stress equilibrium equation for axisymmetric condition in cylindrical coordinate can be expressed as:

$$\left(\frac{1}{r}\sigma_r + \frac{\partial \sigma_r}{\partial r} + \frac{\partial \sigma_z}{\partial z}\right) + \rho_m g = 0 \tag{1c}$$

The assumption of ideal homogeneous and isotropic porous medium leads to Terzaghi's effective stress definition [38]:

$$\sigma = \sigma' + p_f I \tag{2}$$

where σ' is the effective stress tensor, p_f is the pore fluid pressure and I is the identity tensor.

Furthermore, by referring to the principal of thermo-poroelasticity, the increment of elastic volumetric strain tensor in small deformation regime can be expressed as:

$$d\varepsilon_{vol} = \left(\frac{1}{K}\right)d\sigma' - \alpha_d dT \tag{3}$$

where K is the drained bulk modulus of a medium. α_d is the isotropic thermal expansion which is assumed to be equal to linear thermal expansion coefficient of solid grains(α_s), and T is temperature. In Eq. (3) contraction is positive and expansion is negative.

Considering axisymmetric condition of the problems ($\partial q_\varphi / \partial \varphi = 0$), the mass balance of water phase in transient condition in cylindrical coordinates can be expressed as:

$$\frac{\partial m_f}{\partial t} + \rho_f \left(\frac{1}{r}q_r + \frac{\partial q_r}{\partial r} + \frac{\partial q_z}{\partial z}\right) = 0 \tag{4}$$

where

$$m_f = n\rho_f \tag{5a}$$

$$q_r = -\frac{k}{\mu}\frac{\partial p_f}{\partial r} \tag{5b}$$

$$q_z = -\frac{k}{\mu}\left(\frac{\partial p_f}{\partial z} + \rho_f g\right) \tag{5c}$$

m_f is the water mass fraction in the medium. In Eqs. (5b) and (5c), q_r and q_z are water fluxes governed by Darcy's law, k and μ are intrinsic permeability of the soil and dynamic viscosity of the fluid, respectively.

The energy balance equation is coupled with the mass balance equations in order to update the medium temperature in each time step during the thermal loading and recovery time. Energy balance is shown
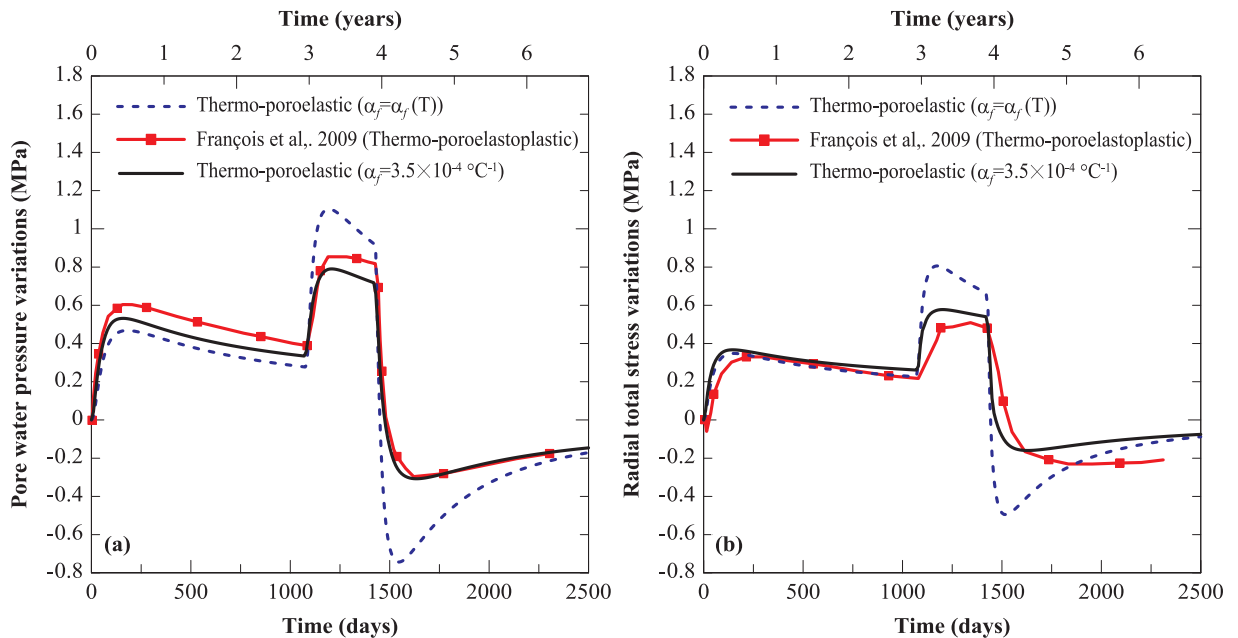

Fig. 9. The variation of (a) thermal pressurization and, (b) radial total stress, with time at the observation borehole (r = 1.515 m from the heater): the comparison between the current model (constant and temperature dependent thermal expansion coefficient of water) and Thermo-poroelastoplastic model [33].
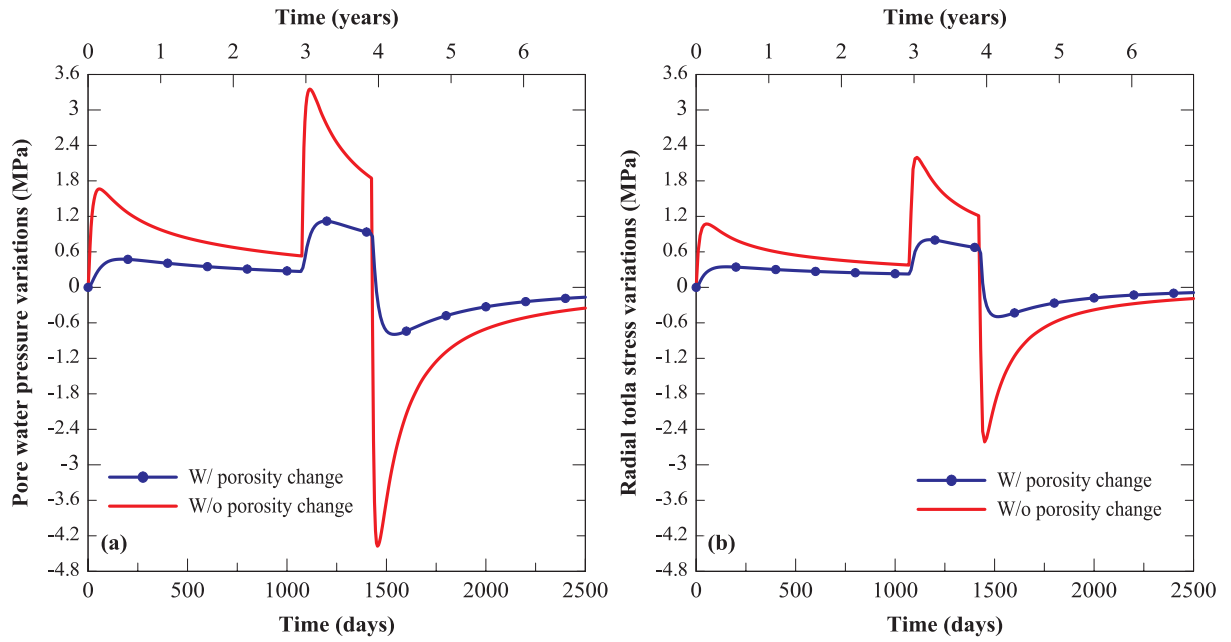
Fig. 10. Comparison of the (a) thermal pressurization and, (b) radial total stress evolutions versus time with and without considering porosity change.
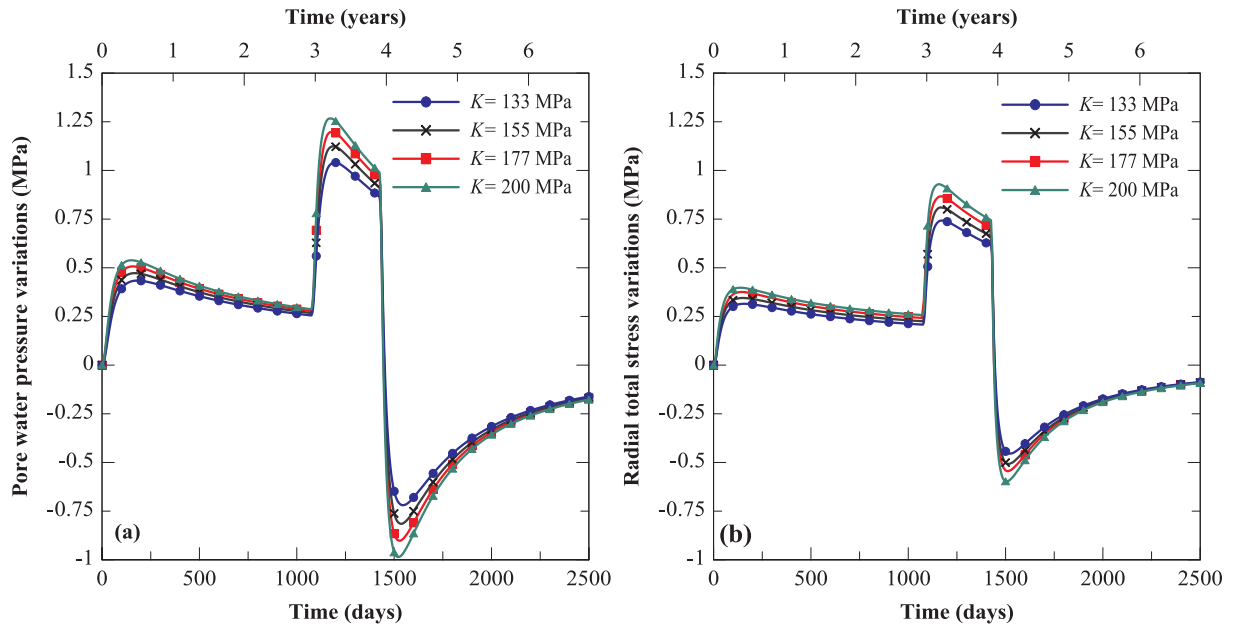

Fig. 11. Comparison of the (a) thermal pressurization and, (b) radial total stress evolutions versus time with considering different drained bulk moduli.

in Eq. (6). Note, $\partial T / \partial \varphi = 0$ for axisymmetric condition.

$$\frac{\partial T}{\partial t} + \frac{(\rho C)_f}{(\rho C)_m} \left[q_r \left(\frac{1}{r} T + \frac{\partial T}{\partial r} \right) + q_z \frac{\partial T}{\partial z} \right] = \alpha_m \left(\frac{1}{r} \frac{\partial T}{\partial r} + \frac{\partial^2 T}{\partial r^2} + \frac{\partial^2 T}{\partial z^2} \right) + Q$$

(6)

where Q is the heat source/sink.

$$(\rho C)_m = n \rho_f C_f + (1 - n) \rho_s C_s$$

(7a)

$$\alpha_m = \frac{\lambda_m}{(\rho C)_m}$$

(7b)

$$\lambda_m = n \lambda_f + (1 - n) \lambda_s$$

(7c)

where C_m, C_f, and C_s are the specific heat capacities of the medium, water, and solid grains at constant stress, respectively. λ_m, λ_f, and λ_s are the thermal conductivities of the medium, water, and solid grains,

respectively, and α_s is thermal diffusivity of the medium.

In Eq. (6), the second term on the left side is the heat convection term, and the first term on the right side is governed by Fourier's law of heat conduction. It is worth noting that in most of the heat transfer problems in the geotechnical field, heat convection under hydrostatic condition is disregarded.

The field Eqs. (1c), (4), and (6) which include pore fluid pressure, temperature, and deformation as field variables should be solved simultaneously to model the THM process. Temperature gradient induces thermal strain and pore water pressure. However, only a few studies considered two-way coupling, in which the stress state and updated soil and fluid properties, like porosity and permeability, change the heat transfer rate and soil temperature increments [8,39,40]. While the Eqs. (3) and (6) present the effects of temperature on soil volumetric deformation and effective stress, additional state variable equations are
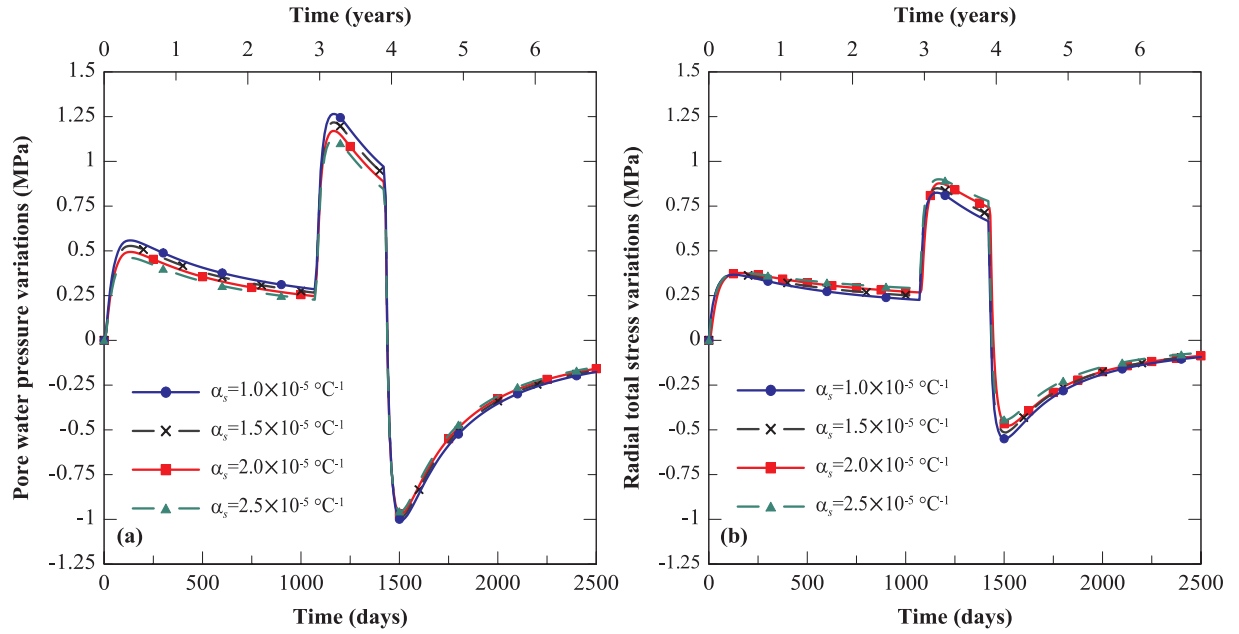
Fig. 12. Comparison of the (a) thermal pressurization and, (b) radial total stress evolutions versus time with considering different thermal expansion coefficients of solid grains.

Table 3
Properties of soil for parametric study.

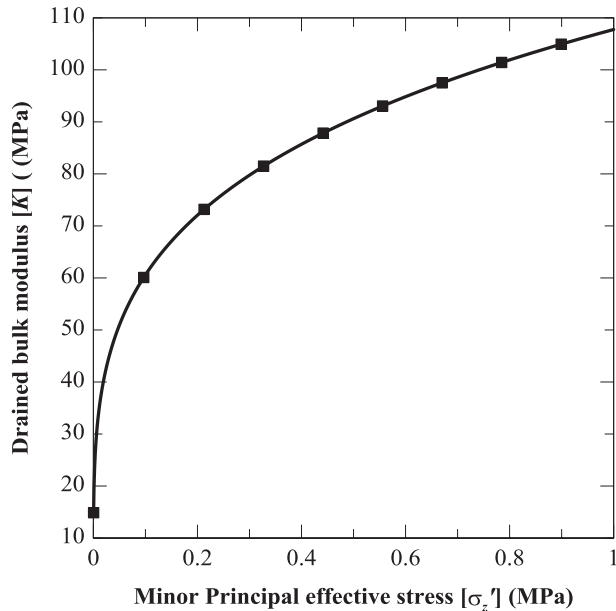| Parameters (dimensions)	Values
ρ_{f0} (kg/m^3)	1000
ρ_s (kg/m^3)	2650
n_o	0.35
ν	0.2
λ_s (W/m·°C)	2.5
C_s (J/kg·°C)	810
α_s (1/°C)	3.0×10^{-5}
T_o (°C)	15

Fig. 13. Variations of drained bulk modulus as a function if minor principal effective stress after Byrne et al. [55].

needed in order to study fluid mass conservation considering soil deformation and temperature increments [38]. Eqs. (8) and (9) express the variations of fluid density and medium porosity with temperature, pore pressure, and effective stress:

$$\frac{\partial \rho_f}{\partial t} = \rho_f \left[\left(\frac{1}{K_f} \right) \frac{\partial p_f}{\partial t} - \alpha_f \frac{\partial T}{\partial t} \right] \tag{8}$$

$$\frac{\partial n}{\partial t} = (1-n) \left[\left(\frac{1}{K} \right) \frac{\partial \sigma'}{\partial t} - \alpha_s \frac{\partial T}{\partial t} \right] \tag{9}$$

where K_f and α_f are the bulk modulus and thermal expansion coefficient of water, respectively. Eq. (9) is obtained from the macroscopic mass balance equation pertaining to solid grains. By substituting Eqs. (8) and (9) in Eq. (5a), and replacing m_f in Eq. (4), the water mass conservation equation is coupled with temperature and deformation fields in a transient state.

$$\frac{\partial p_f}{\partial t} + \frac{1}{S} \left(\frac{1}{r} q_r + \frac{\partial q_r}{\partial r} + \frac{\partial q_z}{\partial z} \right) = \Lambda \frac{\partial T}{\partial t} - \frac{1}{S} \left(\frac{1-n}{K} \right) \frac{\partial \sigma'}{\partial t} \tag{10a}$$

$$S = \frac{n}{K_f} \tag{10b}$$

$$\Lambda = \frac{n\alpha_f + (1-n)\alpha_s}{S} \tag{10c}$$

where Λ, and S are defined as thermal pressurization coefficient and storage coefficient, respectively. Ghabezloo and Sulem [41] defined a similar equation to predict Λ for rocks. Eqs. (8)–(10) indicate that thermal expansion coefficient of the fluid and solids, along with the bulk modulus of water and drained bulk modulus of the porous medium, have a direct effect on thermal pressurization. Therefore, these values and their changes with temperature must be considered in order to accurately predict thermal pressurization.

In addition to fluid density and porosity, other hydraulic and thermal properties of fluid (i.e. water) are considered as temperature dependent. Hence, for careful consideration of these properties, the formulations provided by International Association for the Properties of Water and Steam (IAPWS) are used. The thermodynamic properties of water for the temperature ranging from 10 to 100 °C are calculated based on specific Gibbs free energy, $g(p_f, T)$ and its appropriated
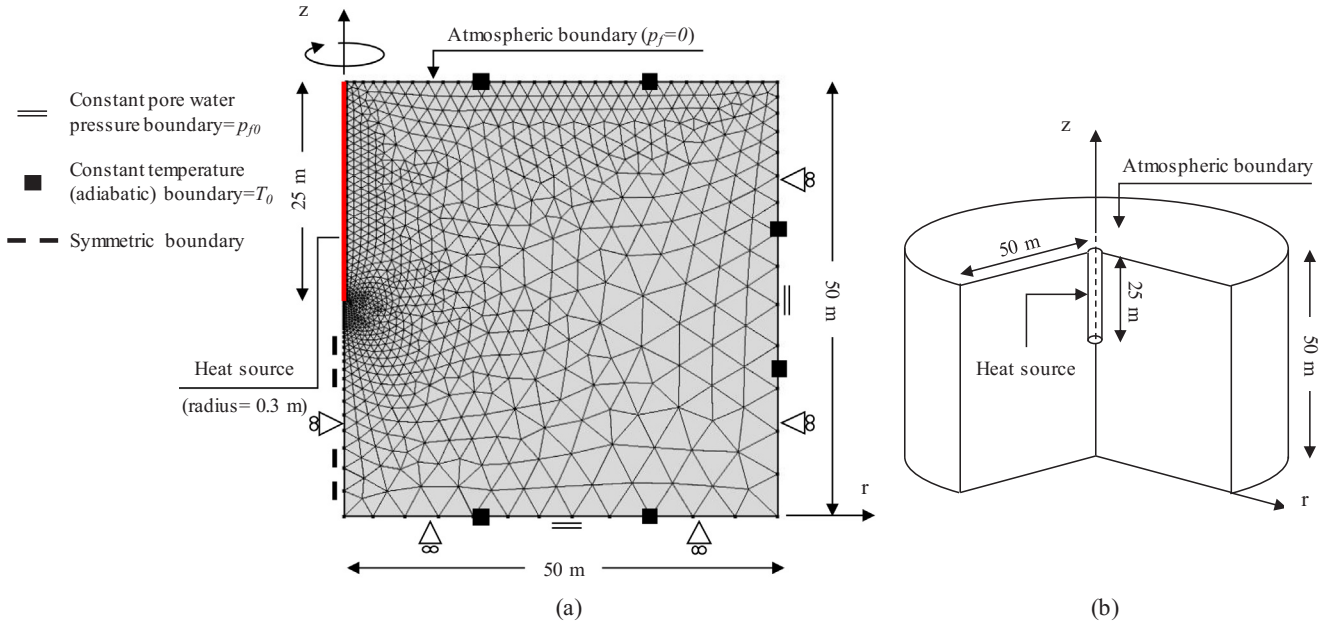
Fig. 14. (a) Finite element mesh of the domain with imposed boundary conditions and, (b) the 3D axisymmetric schematic view of the problem.

Table 4
Parameters considered for the sensitivity study.

Parameters (dimensions)	Values
k_0 (m²)	5×10^{-10}; 1×10^{-10}; 5×10^{-11}; 1×10^{-11}; 5×10^{-12}; 5×10^{-13}; 5×10^{-14}
T_H (°C)	20; 35; 40; 45; 50; 55

derivatives. All the details of the numerical procedure are summarized in [42]. Accordingly, Fig. 1(a), (b), and (c) illustrates the variations of the thermal expansion coefficient, compressibility, dynamic viscosity, heat capacity, and thermal conductivity of water with the temperature ranging from 10 to 100 °C. The temperature values beyond this range are extrapolated.

As it can be seen in Fig. 1(a), the variations of thermal expansion coefficient of water (α_f) with temperature can be as high as 200% when temperature rises from 20 °C to 80 °C; however, in several THM modeling α_f has been considered as constant. Therefore the effects of variable α_f on thermal pressurization, and radial total stress variations is investigated in this paper.

As mentioned earlier, only a few studies have considered the changes in porosity and soil intrinsic permeability to analyze the thermal pressurization and thermal flow in porous media [43]. Results from the current study confirm that even a small variation of the fluid and soil properties (e.g., density, hydraulic conductivity, and porosity) highly affect the overall thermal performance of the porous medium.

Temperature increments induce soil fabric changes and porosity alterations. Pervious research showed intrinsic permeability changes with temperature increments [44]. In this study, the variation of the intrinsic permeability is considered with updated porosity based on the Kozeny-Carman equation (Eq. (11)) [43,45,46]:

$$k = k_0 \left(\frac{1 - n_0}{1 - n} \right)^2 \left(\frac{n}{n_0} \right)^3$$

(11)

where k_0 and n_0 are the initial intrinsic permeability and initial porosity, respectively.

For the quasi-steady state condition where $\partial T/\partial t = \partial m_f/\partial t = 0$, the fluid mass balance equation (Eq. (4)) reduces to:

$$\frac{1}{r} q_r + \frac{\partial q_r}{\partial r} + \frac{\partial q_z}{\partial z} = 0$$

(12)

In this case, the variation of fluid density only makes a change in the gravitational term of Eq. (5c). This condition is explained by the Boussinesq approximation [47]:

$$\rho_f = \rho_{f_0} \left[1 - \alpha_f (T - T_0) \right]$$

(13)

Eq. (13) implies that, in a quasi-steady state where the build-up pore water pressure is diffused due to heating, pore fluid flow can happen because of variations in fluid density. It is worth mentioning that considering Boussinesq approximation in transient heat and mass transfer problems can lead to erroneous solutions [10].

Fig. 2 summarized the coupled Thermo-poro-mechanical model for a saturated porous media. Temperature variations affect the thermal properties of the fluid and hydraulic properties of the soil mixture. Moreover, temperature variations may induce thermal elastic and/or plastic deformations. The thermal deformation alters the porosity and consequently changes the intrinsic permeability. While porosity variations and thermal expansion of fluid can directly affect the thermal pressurization, changes in intrinsic permeability may influence the fluid diffusion. Permeability dictates the rate of dissipation of the thermally-induced pore pressure. Also, changes in porosity affect the storage of heat capacity, and thermal conductivity in balance of energy. Moreover, variations of fluid density due to the temperature changes may cause fluid advection considering Boussinesq approximation. Fluid advection participates in heat convection and changes heat transfer in the soil media in quasi-steady state condition. Here, thermo-poroelastic model has been adopted to simulate a fully coupled THM process in saturated soil. No thermal plastic deformation is considered in this study; the current model is relatively simpler and more practical compared to an advance thermo-elastoplastic constitutive models such as ACMEG-T [28] in which the effect of temperature on preconsolidation pressure and thermal softening of a bounding yield surface are considered. In order to accurately model the heat transfer mechanism and predict the thermo-poro-mechanical behavior of the porous media, the variation of soil and fluid properties with temperature must be considered. In the following section, the results from the current study are compared with analysis of François et al. [33] who used an advanced thermo-poroelastoplastic model (ACMEG-T) with considering constant thermal expansion coefficient of fluid. The comparison with Field
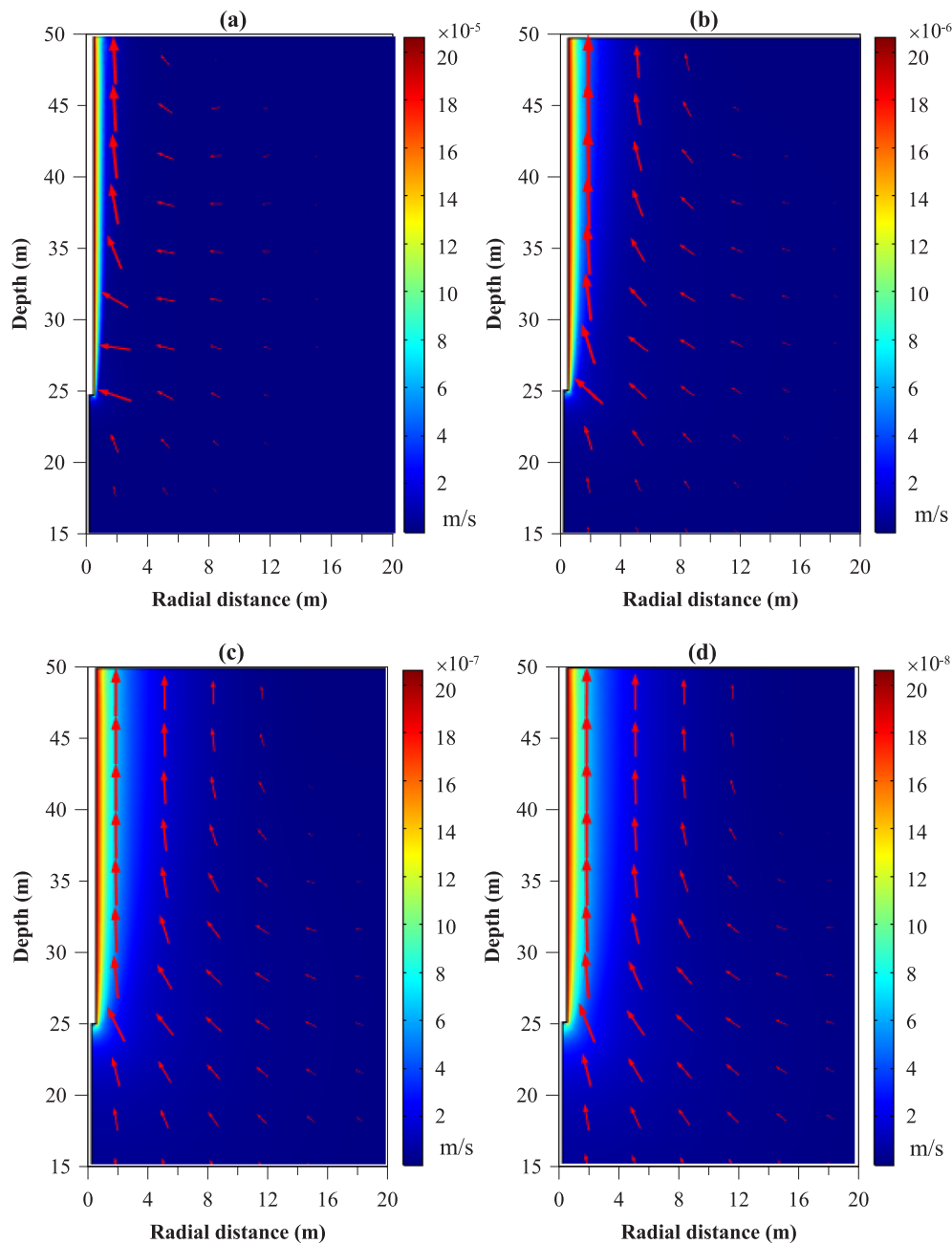
Fig. 15. Pore fluid flow contours close to the heat source ($=50\,°C$) for different permeability values: (a) $5 \times 10^{-10}\,m^2$, (b) $5 \times 10^{-11}\,m^2$, (c) $5 \times 10^{-12}\,m^2$, (d) $5 \times 10^{-13}\,m^2$.

observations confirm the advantages of the current model.

3. Numerical simulations

3.1. ATLAS experiment

The developed thermo-poro-mechanical model is used to analyze the thermally induced pore pressure in a long-time transient state. The underground research facility HADES-URF (Fig. 3), in which the ATLAS test was conducted, was designed and built in Mol, Belgium at a depth of 223 m in Boom clay. The experimental facility was designed to study the THM response of the soil exposed to a radioactive waste deep geological repository [33]. The Boom clay is a deposit of over-con-solidated clay which is considered as a host rock for the Belgian dis-posal of radioactive waste. The ATLAS experiment consists of a hor-izontal main borehole (19 m long) with heaters and two parallel

boreholes (15.65 m long) with instrumentation. The Observation boreholes for measurement have been drilled at 1.184 m and 1.515 m of the main borehole in the same horizontal plane. The changes in tem-perature, pore water pressure, and radial stress have been measured in observation boreholes [35].

Fig. 4 presents the thermal loading in the main borehole. The first heating phase started on July 1993 at a power of 900 W and lasted about 3 years. The second heating phase started in June 1996 at full power (1800 W) for almost a year. The cooling phase begin in May 1997 by turning off the heaters [35]. The thermal loading used in this study borrowed exactly from the field while the thermal loading con-sidered in François et al. [33] had higher thermal power in heating phases.

Several researchers studied the evaluation of thermal and mechan-ical properties of Boom clays [19,48–51]. The properties of the Boom clay used in this study are selected according to the reported properties
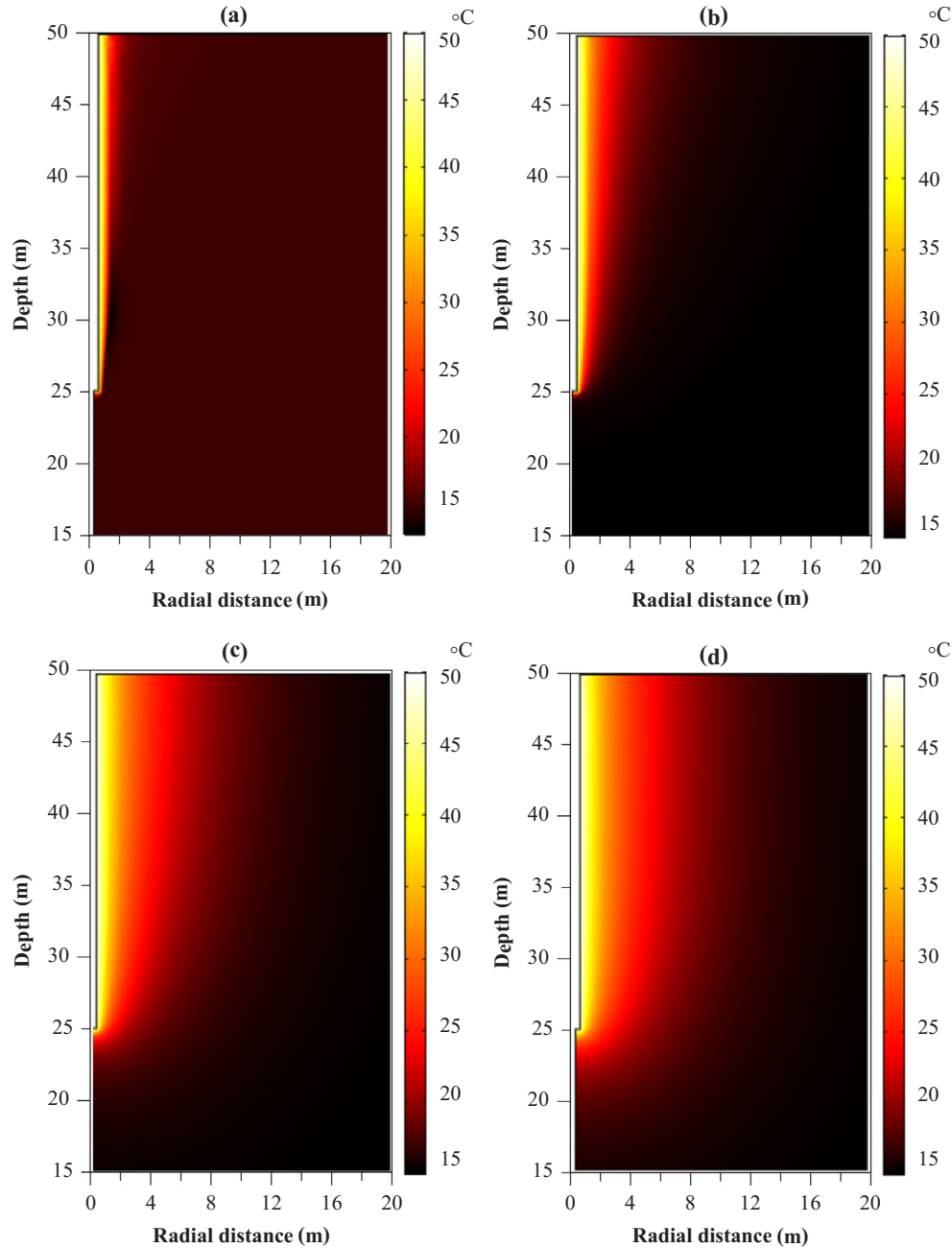
Fig. 16. Heat propagation close to the heat source ($=50\,°C$) for different permeability values: (a) $5 \times 10^{-10}\,\text{m}^2$, (b) $5 \times 10^{-11}\,\text{m}^2$, (c) $5 \times 10^{-12}\,\text{m}^2$, (d) $5 \times 10^{-13}\,\text{m}^2$.

ofBoom clay for the ATLAS project in literature (see Table 1).

3.2. Numerical setup and conditions

A 2D axisymmetric domain in the horizontal plane is considered with the heat source on the symmetry boundary. Calibration results showed the effect of boundary conditions on the analysis is negligible when the radial and perpendicular distances of 100 m from the heater are considered. The geometry is in agreement with the THM numerical analysis performed by François et al. [33].The in-situ stress, initial pore water pressure, and temperature are reported in Table 2.

Constant temperature and pore pressure equal to the initial values are considered for all boundaries except the axisymmetric boundary. The perpendicular displacement to the boundaries is prevented. The geometry and finite element mesh with the boundary conditions along

with the 3D schematic view of ATLAS experiment are shown in Fig. 5. In the numerical simulations, the solutions of partial differential equations are obtained using direct linear solver in COMSOL with fully coupled approach where the relative tolerance is set to 0.01%.

3.3. Results and discussion

The comparison between the results obtained from the current study, experiment, and thermo-poroelastoplastic analysis of François et al. [33] are presented in Figs. 6–8. All the results shown in Figs. 6–8 were monitored at 1.515 m from the heat source at the observation borehole. Fig. 6 shows the temperature variations for 2500 days (6.8 years) including two heating phases and one cooling cycle according to Fig. 4. The numerical results are in good agreement with experiment data while no adjustment was made for the thermal power
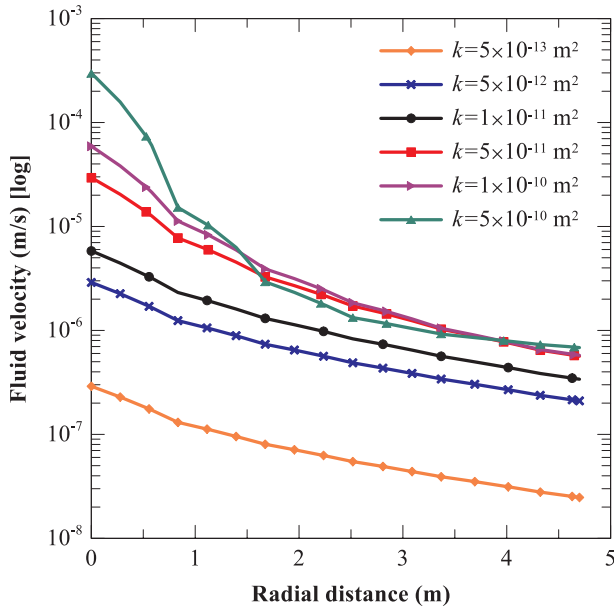
Fig. 17. Fluid velocity variations in radial distance in semi-log plane for different permeability values (T_H = 45 °C).

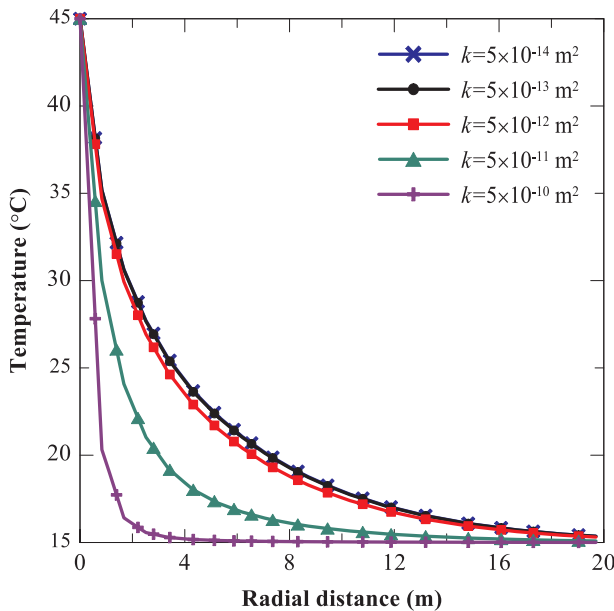**Fig. 18.** Temperature variations in radial distance for different permeability values (T_H = 45 °C).

at the heater level. Fig. 7 shows the comparison of thermal pressurization variations obtained in this study with experimental data and results of thermo-poroelastoplastic analysis from François et al. [33]. As it is evident in Eq. (10c), thermal pressurization is mainly due to the difference between the thermal expansion coefficient of water and solid grains. The magnitude of thermal pressurization inversely depends on compressibility of pressurized fluid and medium. It can be concluded that in shallower depths where the compressibility of the soil is higher, the effect of temperature on fluid pressure is less evident. Moreover, another controlling parameter for thermal pressurization is the intrinsic permeability of the porous medium which governs how fast the excessive pore pressure can dissipate. Therefore, pressurization is more likely to happen in less compressible and very low permeability soils or rocks.

In Fig. 7, the overall trend of the results is a reasonable match with

experimental data. While the obtained thermal pressurization is underestimated during the first phase of the heating, the maximum pressure at the second phase of the heating has been captured well with the current model. Moreover, the predicted negative pressurized pore water during the cooling phase matches with field observations. In general, the thermal pressurization is predicted reasonably well during the thermal loading. Note that the current model is simpler and more practical than the advanced THM model used by François et al. [33].

Fig. 8 represents the variations of total radial stress (σ_r) with time. Although the current model matches better with the field observations, both models are not capturing the variations of total radial stress observed in the field. One scenario is that the total radial stress recorded by the instrument at the observation borehole might have been affected by high temperature. François et al. [24] and Bernier and Neerdael [43] discussed this issue in more detail.

As previously mentioned, the thermal pressurization is due to the difference of thermal expansion coefficients of water and solid grains; hence, we postulate that thermal expansion coefficients of water, which is highly temperature depended, may be the key parameter in this matter. In Fig. 9(a) and (b), the reason of discrepancy in thermal pressurization and radial total stress simulations between the current and thermo-poroelastoplastic model is shown by setting a constant value for the thermal expansion coefficient of water (equal to the value used in François et al. [33]) in the current model. It should be noted that no external mechanical loading is applied in this problem and variations of total stress are strongly affected by thermal loading through pore pressure changes. The results of thermal pressurization and radial total stress with the constant thermal expansion coefficient match well with the thermo-poroelastoplastic model. In conclusion, it is interesting to note that, utilizing realistic fluid parameters can have great effects on heat-induced pore pressure.

Fig. 10(a) and (b) compares the results of the thermal pressurization and radial total stress evolutions versus time with and without considering porosity variations. According to Eq. (9), the maximum porosity change (no volumetric plastic defamation is considered) during the thermal loading is $\Delta n = +0.24\%$ for the second heating phase and $\Delta n = -0.11\%$ for the cooling phase. Even though porosity variations are very small, it is shown that neglecting the porosity changes in soil medium results in enormous error in the predictions of thermal pressurization and radial total stress.

As it can be seen in Eq. (9) different bulk moduli, and thermal expansion coefficient of solid grains result in different porosity variations and it is expected that variations of these parameters alters thermal pressurization, and total stress. Figs. 11 and 12 depict the evolution of thermal pressurization and radial total stress with respect to different drained bulk moduli and thermal expansion coefficients of solid grains, respectively. In Fig. 11(a) and (b), larger drained bulk modulus results in higher variations in thermal pressurization and radial total stress in all heating and cooling phases. Fig. 11 shows increasing bulk modulus from 133 MPa to 200 MPa results in 22% higher thermal pressurization in the second heating phase and 37% reduction in pore water pressure in the cooling phase.

In Fig. 12(a) and (b), linear thermal expansion coefficients of solid grains are considered such that it represent different clayey soils [52–54]. Fig. 12(a) shows that higher thermal expansion coefficient results in slightly lower thermal pressurization (less than 7% when the thermal expansion coefficient of solid grans increases from $1 \times 10^{-5}\,°C^{-1}$ to $2 \times 10^{-5}\,°C^{-1}$) while in Fig. 12(b) this effect is reversed for radial total stress variations in the first two heating phases. It is worth mentioning that the effect of temperature variations on total stress is not only through the thermal pore pressurization but is also due to the direct effect of thermal deformation on the total stress.

The results from the current study shows a simple thermo-elastic model can be used to predict the thermal pressurization, and total stress variations close to heat sources if temperature dependent properties of soil and fluid are considered. Please note, further research is needed to
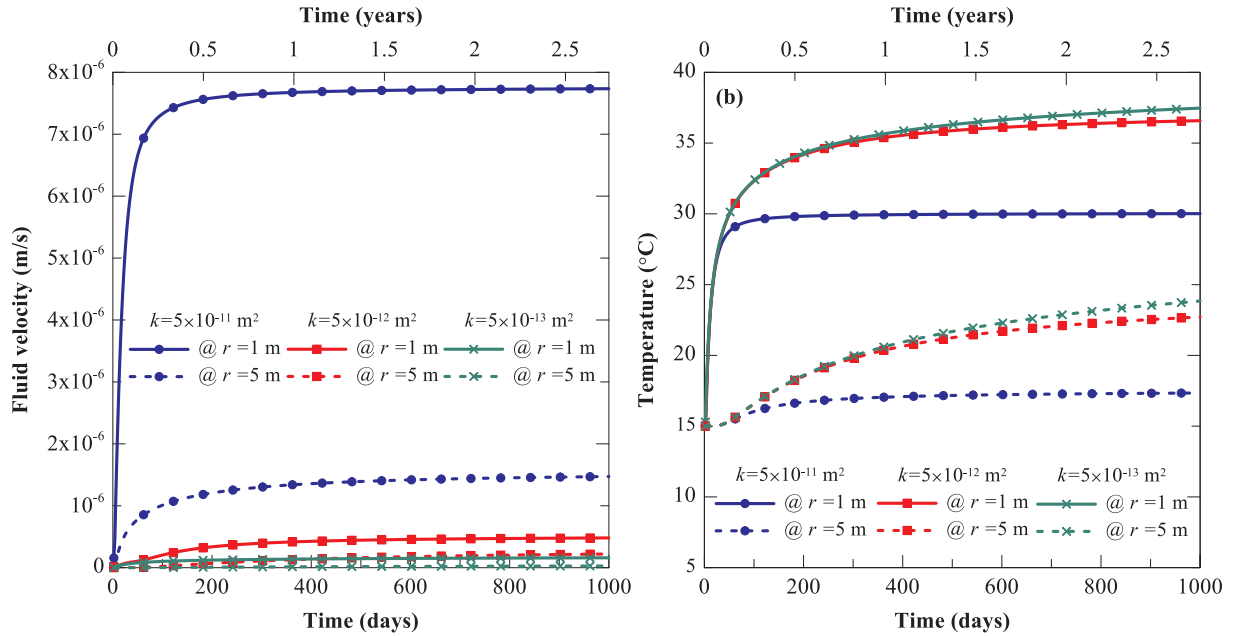
Fig. 19. The evolution of (a) fluid velocity and (b) temperature, versus time for different permeability values (T_H = 45 °C).

analyze the difference in total strain and displacement considering thermo-elastic model with variable parameters compare to an advanced thermo-elastoplastic model. In order to accurately predict thermal stress and strain, advanced thermo-elastoplastic model with considering temperature dependent properties might be needed.

3.4. Parametric study for soil with higher permeability

In this section, a parametric study is conducted to evaluate the influence of different values of intrinsic permeability (i.e. different types of soil) and heat source temperature on heat induced-pore fluid pressure and heat-induced pore fluid flow. Only a constant thermal load for each analysis is considered to ensure that a quasi-steady state condition can be reached (i.e. sufficient time for thermal and hydraulic diffusion). The soil medium is in range of sandy soil to silty sands to study the mass and heat transfer in high permeability soils. As was expected, thermal pressurization is negligible as it can be diffused so fast. Furthermore, for the zones close to the ground surface (range of 25 m below the ground surface), the effect of confining pressure is less tangible.

3.5. Numerical setup and conditions

The thermal and hydraulic properties of the medium are reported in Table 3. In addition, the drained bulk modulus of the medium is considered to be stress dependent and is defined as follows [55]:

$$K = k_B P_a \left(\frac{\sigma_z'}{P_a} \right)^{0.25} \tag{14}$$

where K_B represents the relative density of sands and is set to be 600 for this study, and P_a is the atmospheric pressure. The variations of drained bulk modulus with minor principal effective stress are shown in Fig. 13.

In order to perform a parametric study at the quasi-steady state condition, 2D axisymmetric model with the heat source vertically placed on the symmetry axis is considered. The domain of the simulation is selected to be 50 × 50 m to avoid the effects of boundary conditions. Initial stress and pore pressure values are generated with consideration of gravity, and the initial temperature of the medium is assumed to be 15 °C. The perpendicular displacement is prevented on all boundaries except the left boundary (axisymmetric axis). Hydrostatic pore pressure is considered for top, right, and bottom

boundaries, and no flow condition is considered for the axisymmetric axis. Adiabatic temperature is imposed on right and bottom boundaries while thermal insulation is set at the ground surface. The 2D axisymmetric finite element mesh and boundary conditions along with the 3D axisymmetric schematic view of the domain are shown in Fig. 14.

The parametric study is performed with different values of temperature and initial intrinsic permeability (see Table 4). Please note, temperature ranges are selected such that they represent the heating phase of the ground close to energy piles.

3.6. Results and discussion

The THM numerical simulation is carried out for 1000 days (2.7 years) with respect to the initial and boundary conditions described in the previous section. The results of the parametric study are shown in Figs. 15–19. Fig. 15(a) through (d), demonstrates the velocity contours after reaching the quasi-steady state condition for different permeability values [$k = 5 \times (10^{-10}, 10^{-11}, 10^{-12}, 10^{-13})$ m²] where $T_H = 50$ °C. Note, numerical results only presented for the small zone around the heat source. The red arrows show the direction of the flow. As can be seen in the figures, fluid flow moves towards the heat source and upwards. As the changes in pore water pressure are negligible in high permeability media (the highest change is $\Delta p_f = 3$ kPa which diffuses rapidly), fluid flow occurs due to changes in the water density in the gravitational term of Darcy's flow around the heat source according to Eq. (13). As expected, the velocity decreases for low permeable soil. Although the pore fluid velocity is small, it can have a significant effect on the heat transfer rate at the quasi-steady state condition. Fig. 16(a) through (d), shows the heat propagation around the heat source for an identical thermal loading with different permeability values. Interestingly, Fig. 16(a) and (b) show smaller heat propagation comparing to case (c) and (d), where it has lower permeability. This phenomenon can be interpreted as dominant heat convection caused by heat-induced pore fluid flow which is acting against the heat conduction. As the pore water flows towards the heat source (due to fluid density gradient), it prevents the heat flowing away from the heat source. In other words, heat convection dominates the heat conduction mechanism.

The fluid velocity changes with radial distance for different conditions are presented in Fig. 17. As can be seen in the figure, the zone influenced by heat-induced pore fluid flow is happening in the range of

2–4 m from the heat source (see Fig. 17). The fluid velocity reduction slope for $k = 5 \times 10^{-10}$ m^2 is higher than other cases with respect to radial distance. The reason is that only a small neighboring zone around the heat source is influenced by elevated temperature in high permeable soil.

However, in order to quantify the effect of thermally-induced pore fluid flow in the heat transfer mechanism in high permeable soil, soil temperature with radial distance for different permeability values are compared. Fig. 18 shows the temperature values for a large range of permeability values with respect to radial distance. As can be observed, the temperature propagation in radial distance is lower in soils with high permeability. As the permeability decreases, the heat propagates further from the pile. For very low permeable soils, heat convection becomes negligible and heat conduction plays the sole role in the media. Fig. 18 demonstrates that the permeability threshold in which temperature induces pore fluid flow for this specific condition is in the range of $k = 5 \times 10^{-10}$ m^2.

Fig. 19(a) and (b) is illustrating the evolution of fluid velocity and temperature, respectively, versus time for different permeability values. The measuring points are at the mid depth of the heat source and at r = 1 and 5 m. According to Fig. 19(a), the induced velocity for high permeable soil is eight times higher for the zones closer to the heat source (e.g., r = 1 m) compared to farther areas (e.g., r = 5 m). Higher fluid flow indicates that heat-induced fluid flow is stronger where temperature increments are significant. Such a difference is not considerable for the lower permeability value. Fig. 19(b) presents that the effect of permeability on temperature increments at both closer and farther zones is considerable. Moreover, when the permeability is higher, the temperature reaches the nearly steady-state condition faster than in lower permeable soil. In addition, the temperature difference for two cases ($k = 5 \times 10^{-11}$ m^2 and $k = 5 \times 10^{-12}$ m^2) is roughly 22% and 31%, respectively, for r = 1 m and r = 5 m at the steady-state condition. Results which are presented in Figs. 15–19 confirm that the effect of thermally-induced pore fluid flow on the heat transfer mechanism is inevitable and it cannot be ignored for permeability higher than $k = 5 \times 10^{-12}$ m^2 for temperature ranges presented in this study (20–55 °C). It is worth mentioning that, according to the numerical analysis performed by Delaney [6], heat convection can happen in soil with permeability values as low as k = 2.03×10^{-16} m^2 at the depths of 0.1–5 km and temperature variation of 500–1000 K.

4. Conclusion

Two common cases of heat transfer in soils are simulated and analyzed numerically using the thermo-poro-mechanical model in transient and quasi-steady state conditions. The effects of different thermal and hydraulic parameters are considered and assessed in detail. Among all these parameters, the effect of variations of porosity and the thermal expansion coefficient of water on thermal pressurization, and radial total stress and the fluid density variation on heat-induced fluid flow at the quasi-steady state condition turned out to be paramount.

According to the numerical results presented in this study, it can be concluded that THM mechanism in high and low permeable soils are different; for low permeable soil, temperature increments result in thermal pressurization, while for soils with high permeability values (sand or silty-sand) temperature increments result in thermally-induced pore fluid flow, and thermal pressurization becomes negligible. In order to perform THM modeling and accurately predict the thermal pressurization and radial total stress, changes in soil and fluid properties with temperature and pressure must be considered. Intrinsic permeability plays an important role on the coupling effect between heat-induced pore fluid flow and thermal convection. It is observed that, in higher values of permeability in which heat convection is dominant and acting on opposite to heat conduction, heat accumulates close to the heat source. We also find that for high permeable soil (k ≥ 5×10^{-12} m^2) and for temperature ranges of 20–55 °C, it is necessary to consider the thermally induced pore fluid flow to accurately predict heat transfer mechanism in soil media.

References

[1] Schubert G, Straus JM. Three-dimensional and multicellular steady and unsteady convection in fluid-saturated porous media at high Rayleigh numbers. J Fluid Mech 1979;94(1):25–38.

[2] Jiménez-Islas H, López-Isunza F, Ochoa-Tapia J. Natural convection in a cylindrical porous cavity with internal heat source: a numerical study with Brinkman-extended Darcy model. Int J Heat Mass Transf 1999;42(22):4185–95.

[3] Hossain MA, Wilson M. Natural convection flow in a fluid-saturated porous medium enclosed by non-isothermal walls with heat generation. Int J Therm Sci 2002;41(5):447–54.

[4] Kalabin E, Kanashina M, Zubkov P. Heat transfer from the cold wall of a square cavity to the hot one by oscillatory natural convection. Numer Heat Transf Part A: Appl 2005;47(6):609–19.

[5] Hossain M, Saleem M, Saha SC, Nakayama A. Conduction-radiation effect on natural convection flow in fluid-saturated non-Darcy porous medium enclosed by non-isothermal walls. Appl Math Mech 2013;34(6):687–702.

[6] Delaney PT. Rapid intrusion of magma into wet rock: groundwater flow due to pore pressure increases. J Geophys Res Solid Earth 1982;87(B9):7739–56.

[7] Lee T-C, Delaney PT. Frictional heating and pore pressure rise due to a fault slip. Geophys J Int 1987;88(3):569–91.

[8] Bonafede M, Mazzanti M. Hot fluid migration in compressible saturated porous media. Geophys J Int 1997;128(2):383–98.

[9] Anderson MP. Heat as a ground water tracer. Groundwater 2005;43(6):951–68.

[10] Ingebritsen S, Geiger S, Hurwitz S, Driesner T. Numerical simulation of magmatic hydrothermal systems. Rev Geophys 2010:48.

[11] Townsend MR. Modeling thermal pressurization around shallow dikes using temperature-dependent hydraulic properties: implications for deformation around intrusions. J Geophys Res Solid Earth 2018;123(1):311–23.

[12] Cherati DY, Ghasemi-Fare O. Analyzing transient heat and moisture transport surrounding a heat source in unsaturated porous media using the Green's function. Geothermics 2019;81:224–34.

[13] Ghasemi-Fare O, Basu P. Predictive assessment of heat exchange performance of geothermal piles. Renew Energy 2016;86:1178–96.

[14] Ghasemi-Fare O, Basu P. Thermally-induced pore pressure fluctuations around a geothermal pile in sand. Geo-Chicago, GSP 2016;270:14–8.

[15] Ghasemi-Fare O, Basu P. Role of thermally induced buoyant flow in altering energy harvesting through geothermal piles. Geotechnical Frontiers 2017, GSP, vol. 280. 2017. p. 113–23.

[16] Ghasemi-Fare O, Basu P. Numerical modeling of thermally induced pore water flow in saturated soil surrounding geothermal piles. IFCEE 2015. 2015. p. 1668–77.

[17] Baldi G, Hueckel T, Pellegrini R. Thermal volume changes of the mineral–water system in low-porosity clay soils. Can Geotech J 1988;25(4):807–25.

[18] Hueckel T, Borsetto M. Thermoplasticity of saturated soils and shales: constitutive equations. J Geotech Eng 1990;116(12):1765–77.

[19] Delage P, Sultan N, Cui YJ. On the thermal consolidation of Boom clay. Can Geotech J 2000;37(2):343–54.

[20] Abuel-Naga HM, Bergado DT, Bouazza A. Thermally induced volume change and excess pore water pressure of soft Bangkok clay. Eng Geol 2007;89(1–2):144–54.

[21] Ghasemi-Fare O, Basu P. Influences of ground saturation and thermal boundary condition on energy harvesting using geothermal piles. Energy Build 2018;165:340–51.

[22] Mohajerani M, Delage P, Sulem J, Monfared M, Tang AM, Gatmiri B. A laboratory investigation of thermally induced pore pressures in the Callovo-Oxfordian claystone. Int J Rock Mech Min Sci 2012;52:112–21.

[23] Braun P, Ghabezloo S, Delage P, Sulem J, Conil N. Theoretical analysis of pore pressure diffusion in some basic rock mechanics experiments. Rock Mech Rock Eng 2018;51(5):1361–78.

[24] Joshaghani M, Ghasemi-Fare O, Ghavami M. Experimental Investigation on the effects of temperature on physical properties of sandy soils. IFCEE 2018. 2018. p. 675–85.

[25] Campanella RG, Mitchell JK. Influence of temperature variations on soil behavior. J Soil Mech Found Div 1968.

[26] Hueckel T, Pellegrini R. Effective stress and water pressure in saturated clays during heating–cooling cycles. Can Geotech J 1992;29(6):1095–102.

[27] Cui YJ, Sultan N, Delage P. A thermomechanical model for saturated clays. Can Geotech J 2000;37(3):607–20.

[28] Laloui L, François B. ACMEG-T: soil thermoplasticity model. J Eng Mech 2009;135(9):932–44.

[29] Başer T, McCartney JS. Transient evaluation of a soil-borehole thermal energy storage system. Renew Energy 2018.

[30] Ghasemi-Fare O, Basu P. Thermal operation of geothermal piles installed in sand—a comparative assessment using numerical and physical models. IFCEE 2015. 2015. p.

1721–30.

[31] Fare GO, Basu P. An annular cylinder source model for heat transfer through energy piles; 2013.

[32] Ghasemi-Fare O, Basu P. A practical heat transfer model for geothermal piles. Energy Build 2013;66:470–9.

[33] François B, Laloui L, Laurent C. Thermo-hydro-mechanical simulation of ATLAS in situ large scale test in Boom Clay. Comput Geotech 2009;36(4):626–40.

[34] Hueckel T, Francois B, Laloui L. Temperature-dependent internal friction of clay in a cylindrical heat source problem. Géotechnique 2011;61(10):831–44.

[35] De Bruyn D, Labat S. The second phase of ATLAS: the continuation of a running THM test in the HADES underground research facility at Mol. Eng Geol 2002;64(2–3):309–16.

[36] Loveridge F, Powrie W. Pile heat exchangers: thermal behaviour and interactions. Proc ICE-Geotech Eng 2013;166(2):178–96.

[37] Fuentes R, Pinyol N, Alonso E. Effect of temperature induced excess porewater pressures on the shaft bearing capacity of geothermal piles. Geomech Energy Environ 2016;8:30–7.

[38] Coussy O. Poromechanics. John Wiley & Sons; 2004.

[39] Moradi A, Smits KM, Lu N, McCartney JS. Heat transfer in unsaturated soil with application to borehole thermal energy storage. Vadose Zone J 2016;15(10).

[40] Tamizdoust MM, Ghasemi-Fare O. Numerical analysis on feasibility of thermally induced pore fluid flow in saturated soils. Eighth international conference on case histories in geotechnical engineering. Philadelphia, Pennsylvania: ASCE; 2019. p. 73–82.

[41] Ghabezloo S, Sulem J. Stress dependent thermal pressurization of a fluid-saturated rock. Rock Mech Rock Eng 2009;42(1):1.

[42] Spang B. Excel add-in for properties of water and steam in SI-units. Water97_v13.xla. Hamburg; 2002.

[43] Chen W, Ma YS, Yu HD, Li XL, Sillen X. Effects of temperature and thermally-induced microstructure change on hydraulic conductivity of Boom Clay. J Rock Mech Geotech Eng 2017;9(3):383–95.

[44] Joshaghani M, Ghasemi-Fare O. A Study on thermal consolidation of fine grained soils using modified triaxial cell. Eighth international conference on case histories in geotechnical engineering. Philadelphia, Pennsylvania: ASCE; 2019. p. 148–56.

[45] Chapuis RP, Aubertin M. On the use of the Kozeny Carman equation to predict the hydraulic conductivity of soils. Can Geotech J 2003;40(3):616–28.

[46] Han G, Dusseault MB. Description of fluid flow around a wellbore with stress-dependent porosity and permeability. J Petrol Sci Eng 2003;40(1–2):1–16.

[47] Nield DA, Bejan A. Convection in porous media vol. 3. Springer; 2006.

[48] Bernier F, Li XL, Bastiaens W. Twenty-five years' geotechnical observation and testing in the Tertiary Boom Clay formation. Géotechnique 2007;57(2):229–37.

[49] Baldi G, Hueckel T, Peano A, Pellegrini R. Developments in modelling of thermo-hydro-geomechanical behaviour of boom clay and clay-based buffer materials. Commission of the European Communities. Nucl Sci Technol 1991.

[50] Horseman S, Winter M, Enwistle D. Geotechnical characterization of Boom clay in relation to the disposal of radioactive waste. Commission of the European Communities; 1987.

[51] Delage P, Le T-T, Tang A-M, Cui Y-J, Li X-L. Suction effects in deep Boom clay block samples. Géotechnique 2007;57(2):239–44.

[52] Ahrens TJ. Mineral physics & crystallography: a handbook of physical constants vol. 2. American Geophysical Union; 1995.

[53] Muñoz J, Alonso E, Lloret A. Thermo-hydraulic characterisation of soft rock by means of heating pulse tests. Géotechnique 2009;59(4):293–306.

[54] Baldi G, Borsetto M, Hueckel T. Calibration of mathematical models for simulation of thermal, seepage and mechanical behaviour of Boom clay: Final report, EUR 10924 EN; 1987.

[55] Byrne PM, Cheung H, Yan L. Soil parameters for deformation analysis of sand masses. Can Geotech J 1987;24(3):366–76.